Colloids and Surfaces A: Physicochem. Eng. Aspects 401 (2012) 116–125

Contents lists available at SciVerse ScienceDirect

Colloids and Surfaces A: Physicochemical and Engineering Aspects

journal homepage: www.elsevier.com/locate/colsurfa

Comparison and understanding of the different simulated sunlight photocatalytic activity between the saturated and monovacant Keggin unit functionalized titania materials

Fengyan Ma[a], Tian Shi[a], Jie Gao[b], Ling Chen[a], Wan Guo[a], Yihang Guo[a,*], Shengtian Wang[a,*]

[a] School of Chemistry, Northeast Normal University, Changchun 130024, PR China
[b] Changchun Institute of Optics, Fine Mechanics and Physics, Chinese Academy of Sciences, Changchun 130033, PR China

ARTICLE INFO

Article history:
Received 25 August 2011
Received in revised form 28 February 2012
Accepted 13 March 2012
Available online 22 March 2012

Keywords:
Polyoxometalates
Titania
Composite material
Synergistic photocatalytic effect
Simulated sunlight photocatalysis

ABSTRACT

The saturated and monovacant Keggin unit functionalized titania materials, $H_3PW_{12}O_{40}/TiO_2$ and $K_7PW_{11}O_{39}/TiO_2$, were prepared by one step sol–gel co-condensation followed by solvothermal treatment. The structure, optical absorption properties, morphology, and porosity of the materials were well characterized. Subsequently, their simulated sunlight photocatalytic activity was evaluated by the degradation and mineralization of dye rhodamine B (RB) and endocrine-disrupting chemical diethyl phthalate (DEP). Special attention was paid to provide direct evidences for the explanation of the different photoexcited electron–hole pair separation rates of the $H_3PW_{12}O_{40}/TiO_2$, $K_7PW_{11}O_{39}/TiO_2$, and pure TiO_2 by the photoelectrochemical experiment; simultaneously, the target active species yielded in the $K_7PW_{11}O_{39}/TiO_2$- and $H_3PW_{12}O_{40}/TiO_2$-catalyzed DEP degradation systems were also investigated by the free radical and hole scavenging experiment. Accordingly, reasons for the photocatalytic activity difference between the $K_7PW_{11}O_{39}/TiO_2$ and $H_3PW_{12}O_{40}/TiO_2$ as well as pure TiO_2 were revealed.

1. Introduction

Photocatalysis has consistently drawn much attention for many environmental challenges facing the modern world since it can provide a simple way to use light to perform chemical transformation [1,2]. Hazardous waste remediation, either in aqueous solutions or air, is the most extensively studied application of photocatalysis. Although it has been proved that TiO_2 is a promising candidate among various photocatalysts, its practical application is limited due to low quantum yield and null visible-light photoresponse [3]. Accordingly, many efforts such as utilizing doping metals, nonmetals, and other conductors with wide or narrow band gaps, reducing the size and changing the morphology of TiO_2, and enlarging the surface area were devoted to further improve the photocatalytic efficiency of TiO_2 [4,5].

Polyoxometalates (POMs) are another class of photocatalytically active materials that have also attracted much attention [6–8]. The unique physical and chemical properties of POMs including molecular and electronic versatility, reactivity, and stability make them ideal photocatalyst candidates. Moreover, POMs share the general photochemical characteristics as that of the semiconductor photocatalysts due to their similar electronic attributes. Suitable light energy excitation of the ligand to metal charge transfer (LMCT) band of POMs can be considered as a parallel process to the band gap excitation of TiO_2. Among all kinds of POM clusters with various structures, the saturated Keggin-type POMs such as $H_3PW_{12}O_{40}$ and $H_4SiW_{12}O_{40}$ are well investigated as the photocatalysts. However, the HOMO–LUMO gap (semiconductor "band gap") of the Keggin unit is higher than that of TiO_2, and they thereby must be photoactivated by the light energy with the excited wavelength lower than 260 nm (LMCT band of the Keggin unit situated at *ca.* 260 nm). As for the solar light, it cannot excite $H_3PW_{12}O_{40}$ or $H_4SiW_{12}O_{40}$ directly since its spectrum onset starts at *ca.* 320 nm. However, polyoxotungstates, regardless of saturated or unsaturated types, are efficient electron trappers. Several groups' research has proved the coupling of polyoxotungstate with TiO_2 can enhance the photocatalytic efficiency of TiO_2-catalyzed reactions due to the strong electron accepting ability of the polyoxotungstate and the transfer of electrons from polyoxotungstate to oxygen species presented in the reaction medium [9,10]. Our previous studies also found this synergistic photocatalytic effect existed between the POM and TiO_2, which retarded the fast recombination of the h_{VB}^+–e_{CB}^- pair and thereby the enhanced photocatalytic activity can be obtained in comparison of pure TiO_2 [11–13]. For examples, $H_3PW_{12}O_{40}/TiO_2$ or $H_6P_2W_{18}O_{62}/TiO_2$ composite prepared by a sol–gel co-condensation method exhibited higher photocatalytic activity under both UV ($\lambda > 254$ nm) and visible-light ($\lambda > 400$ nm) irradiation towards dye degradation compared with bare TiO_2 as

* Corresponding authors. Tel.: +86 431 85098705; fax: +86 431 85098705.
E-mail address: guoyh@nenu.edu.cn (Y. Guo).

0927-7757/$ – see front matter © 2012 Elsevier B.V. All rights reserved.
doi:10.1016/j.colsurfa.2012.03.036

well as the starting POM. More recently, Marcì's group reported that the photocatalytic degradation of 2-propanol under the solar simulating Xe lamp irradiation ($\lambda > 320$ nm) occurred successfully by using $H_3PW_{12}O_{40}$-titania material prepared by a post-synthesized method [14,15].

Up till now the POMs selected for studying the synergistic photocatalytic effect are the saturated Keggin-type polyoxotungstates [16]; moreover, it lacks direct evidences to explain this synergistic effect, especially for the POM/TiO_2 composite materials. In the cases of the unsaturated polyoxotungstates, its contribution to the photocatalytic activity of TiO_2 has seldom been studied. Herein, the saturated and monovacant Keggin unit functionalized TiO_2 composite materials, $H_3PW_{12}O_{40}/TiO_2$ and $K_7PW_{11}O_{39}/TiO_2$, were prepared by one step sol–gel co-condensation followed by solvothermal treatment. And then their heterogeneous photocatalytic behaviors were compared by the degradation and mineralization of dye rhodamine B (RB) and endocrine-disrupting chemical diethyl phthalate (DEP) under the simulated sunlight irradiation. Simultaneously, the direct evidences to explain the synergistic photocatalytic effect between the saturated or monovacant Keggin unit and TiO_2 were provided by the photoelectrochemical experiment; we also paid attention to investigate the target active species yielded in the $K_7PW_{11}O_{39}/TiO_2$- and $H_3PW_{12}O_{40}/TiO_2$-catalyzed DEP degradation systems by the free radical and hole scavenging experiment. The above results are expected to provide a better understanding of the mediated electron-transfer process occurred on the surface of the POM/TiO_2 composites with the assistance of the simulated sunlight.

2. Experimental

2.1. Reagents

Titanium tetraisopropoxide (abbreviated TTIP, 98%) and 12-tungstophosphoric acid ($H_3PW_{12}O_{40}$, 99%) were purchased from Aldrich. Rhodamine B and isopropanol (*i*-PrOH) were purchased from Beijing, China. Diethyl phthalate was purchased from Tianjin Guangfu Fine Chemical Research Institute. $K_7PW_{11}O_{39}$ was prepared based on the literature methods [17,18]. All chemicals were used without further purification. Double distilled water was used throughout the experimental procedures.

2.2. Catalyst preparation

2.2.1. Preparation of the $K_7PW_{11}O_{39}/TiO_2$ and $H_3PW_{12}O_{40}/TiO_2$ powder

Preparation of the $K_7PW_{11}O_{39}/TiO_2$ powder. TTIP (3.6 mL) was dissolved in *i*-PrOH (24 mL) under vigorous stirring at room temperature for 2 h. The desired amount of $K_7PW_{11}O_{39}$ (0.125 g and 0.25 g) was dissolved in water (1 mL) at 333 K. The obtained $K_7PW_{11}O_{39}$ solution was added dropwise into the TTIP/*i*-PrOH solution under vigorous stirring. The resulting mixture was adjusted to pH 5 by acetic acid (1 mol L^{-1}), and then it was stirred at room temperature until the transparent gel was formed. The gel was transferred into an autoclave and heated to 423 K with a heating rate of 2 K min^{-1}, and then the gel was held at this temperature for 48 h. The mixture suffered from the following thermal treatment in air: 333 K for 24 h, 353 K for 12 h, 373 K for 2 h, 393 K for 0.5 h, successively. The product obtained was washed three times with water and ethanol at 333 K for 3 h, respectively. Finally, the product was dried at 333 K for 24 h and denoted as $K_7PW_{11}O_{39}/TiO_2$-x (x represents $K_7PW_{11}O_{39}$ loading in the $K_7PW_{11}O_{39}/TiO_2$-x composite). The preparation route of pure TiO_2 is similar to that of the $K_7PW_{11}O_{39}/TiO_2$ in the absence of $K_7PW_{11}O_{39}$.

Preparation of the $H_3PW_{12}O_{40}/TiO_2$ powder. The preparation route of $H_3PW_{12}O_{40}/TiO_2$ was the same as that of the $K_7PW_{11}O_{39}/TiO_2$ except that using $H_3PW_{12}O_{40}$ (0.25 g) dissolved in HNO_3 (1 mol L^{-1}, 1 mL) to avoid its decomposition. The product was denoted as $H_3PW_{12}O_{40}/TiO_2$-y (y represents $H_3PW_{12}O_{40}$ loading in the $H_3PW_{12}O_{40}/TiO_2$-y composite).

2.2.2. Preparation of the $K_7PW_{11}O_{39}/TiO_2/Ti$ and $H_3PW_{12}O_{40}/TiO_2/Ti$ photoanode

The rectangle titanium (Ti) sheets (size 10 mm × 50 mm, thickness 140 μm, purity > 99.6%) were cleaned ultrasonically in water and alcohol for 10 min, respectively. The cleaned Ti sheets were chemically etched in a mixture of HF, HNO_3, and H_2O for 30 s (HF:HNO_3:H_2O = 1:4:5; v/v/v) followed by rinsing with distilled water and drying in argon flow at room temperature. To obtain some viscosity, the $K_7PW_{11}O_{39}/TiO_2$ or $H_3PW_{12}O_{40}/TiO_2$ suspension coming from the autoclave was stirred vigorously for 3 h at room temperature in an open beaker. The obtained suspension was used for spin-coating Ti sheet at an initial spin rate of 5000 rpm for 6 s and then 2000 rpm for 6 s. After aging at room temperature for 12 h, the $K_7PW_{11}O_{39}/TiO_2$ or $H_3PW_{12}O_{40}/TiO_2$ covered sheets suffered from the subsequent thermal treatment in air: 333 K for 24 h, 353 K for 12 h, 373 K for 2 h and 393 K for 0.5 h, successively. The cooled sheets were washed three times with water and ethanol for 3 h at 333 K, respectively. Finally, the sheets were dried at 333 K for 24 h. For a comparison, TiO_2/Ti photoanode was also prepared by the same process.

The weight of the coated TiO_2, $K_7PW_{11}O_{39}/TiO_2$, or $H_3PW_{12}O_{40}/TiO_2$ on each Ti sheet is 2.0 ± 0.2 mg.

2.3. Catalyst characterization

$K_7PW_{11}O_{39}$ and $H_3PW_{12}O_{40}$ loadings in the composite materials were determined by a Leeman Prodigy Spec ICP-AES. XRD patterns were obtained on a D/max-2200 VPC diffractometer using Cu Kα radiation. TEM, HRTEM, and SAED micrographs were recorded on a JEM-2100F high resolution transmission electron microscope at an accelerating voltage of 200 kV. Nitrogen porosimetry measurement was performed on a Micromeritics ASAP 2020M surface area and porosity analyzer after the samples were outgassed under vacuum at 363 K for 1 h and 423 K for 6 h. UV–Vis/DRS were recorded on a Cary 500 UV–Vis–NIR spectrophotometer. XPS were performed on a VG-ADES 400 instrument with Mg Kα-ADES source at a residual gas pressure of below 10^{-8} Pa. FT-IR spectra were recorded on a Nicolet Magna 560 IR spectrophotometer.

2.4. Photoelectrochemical experiment

Photocurrent measurement was carried out using the conventional three electrode setup connected to an electrochemical station (CH Instrument 660 C, Shanghai Chenhua, China). In this electrochemical system, $K_7PW_{11}O_{39}/TiO_2$/Ti, $H_3PW_{12}O_{40}/TiO_2$/Ti, or TiO_2/Ti (effective area is 4 cm^2) was used as a working photoanode, and a Pt sheet (size 30 mm × 40 mm, purity 99.99%) and an Ag/AgCl (saturated KCl) electrode were used as the counter electrode and reference electrode, respectively. The electrolyte was 0.01 mol L^{-1} Na_2SO_4 aqueous solution (110 mL), and the distance between Ti sheet and Pt sheet was fixed at 30 mm. An external 125 W high-pressure mercury lamp was used as UV light source. The distance between Ti sheet and light source was fixed at 80 mm. The measurements were carried out at a constant potential of +1.0 V to the working photoanode.

Table 1
Main characteristic FT-IR data (cm^{-1}) of the starting $K_7PW_{11}O_{39}$ and $H_3PW_{12}O_{40}$ as well as the $K_7PW_{11}O_{39}/TiO_2$ and $H_3PW_{12}O_{40}/TiO_2$-13.8 materials.

Sample	ν_{as} (P—O)	ν_{as} (W═O_d)	ν_{as} (W—O_c/O_e—W)
$K_7PW_{11}O_{39}$	1090/1040	953	862/806/732
$K_7PW_{11}O_{39}/TiO_2$-8.9	1080/1040	951	817/730
$K_7PW_{11}O_{39}/TiO_2$-13.6	1080/1040	949	812/726
$H_3PW_{12}O_{40}$	1080	984	893/810
$H_3PW_{12}O_{40}/TiO_2$-13.8	1070	966	890/815

2.5. Photocatalytic test

The photocatalytic tests were conducted in a quartz reactor with diameter of 63 mm (consistent with that of the facula of the light resource). The light source (being placed *ca.* 15 cm above the reactor) was provided by a PLS-SXE300 Xe lamp (300 W, Beijing Trusttech Co. Ltd., China) equipped with an IR cut filter to remove most of IR irradiation (680–1100 nm). Consequently, the artificial solar light used here matches well with the natural solar light with main emission from 320 nm to 680 nm (see Fig. S1 of Supplementary Information). The light intensity was adjusted to 150 mW cm^{-2} (1.5 AM) measured by a radiometer (OPHIR, Newport, USA). The suspension containing the solid catalyst (150 mg) and an aqueous RB (25 mg L^{-1}, 100 mL) or DEP (20 mg L^{-1}, 100 mL) solution was poured into the reactor. The suspension was ultrasonicated for 10 min and then stirred in the dark for 60 min to obtain a good dispersion. Subsequently, the Xe lamp was turned on and the photocatalytic degradation reaction was conducted. The acidity of the suspension was neutral, and the system was open to air. The temperature of the suspension was maintained at 303 ± 2 K by circulation of water through an external cooling jacket. At given intervals of irradiation, fixed amounts of reaction solution were taken out, centrifuged and filtrated, and the filtrates were analyzed. Decreases of the concentrations of RB were analyzed by a UV-2100PC spectrophotometer (Beijing, China) at λ = 553 nm; in addition, decreases of the concentrations of DEP were analyzed by a Shimadzu LC-20A high pressure liquid chromatography (HPLC): C_{18} column, UV detector (λ = 227 nm), and acetonitrile/water (80/20, v/v) was used as a mobile phase at a flow rate of 0.9 mL min^{-1}. The detection limit for DEP is lower than 0.05 mg L^{-1}. Changes of total organic carbon (TOC) in DEP and RB degradation systems were monitored by a Shimadzu TOC-500 Total Organic Carbon analysis system.

3. Results and discussion

3.1. Catalyst characterization

3.1.1. Compositional and structural information

The structural integrity of the Keggin unit in the $K_7PW_{11}O_{39}/TiO_2$ and $H_3PW_{12}O_{40}/TiO_2$ composite materials was studied by a FT-IR spectroscopic method. From the results summarized in Table 1 it is found that the characteristic vibrational peaks related to the monovacant or saturated Keggin unit still can be observed after the introduction of $K_7PW_{11}O_{39}$ or $H_3PW_{12}O_{40}$ into the TiO_2 framework. Additionally, the shifts of the vibrational frequencies were observed for both of the composites, indicating the interactions existed between the Keggin unit and TiO_2 framework [11,19]. This interaction also leads to the reduced peak intensities of the $K_7PW_{11}O_{39}/TiO_2$ or $H_3PW_{12}O_{40}/TiO_2$ composite in comparison of the starting $K_7PW_{11}O_{39}$ or $H_3PW_{12}O_{40}$ unit.

The interactions between TiO_2 framework and the saturated or monovacant Keggin unit at the surface of the $H_3PW_{12}O_{40}/TiO_2$ or $K_7PW_{11}O_{39}/TiO_2$ composite are further studied by XPS surface probe technique, and the resulting spectra show interesting information about the surface properties of the composite materials

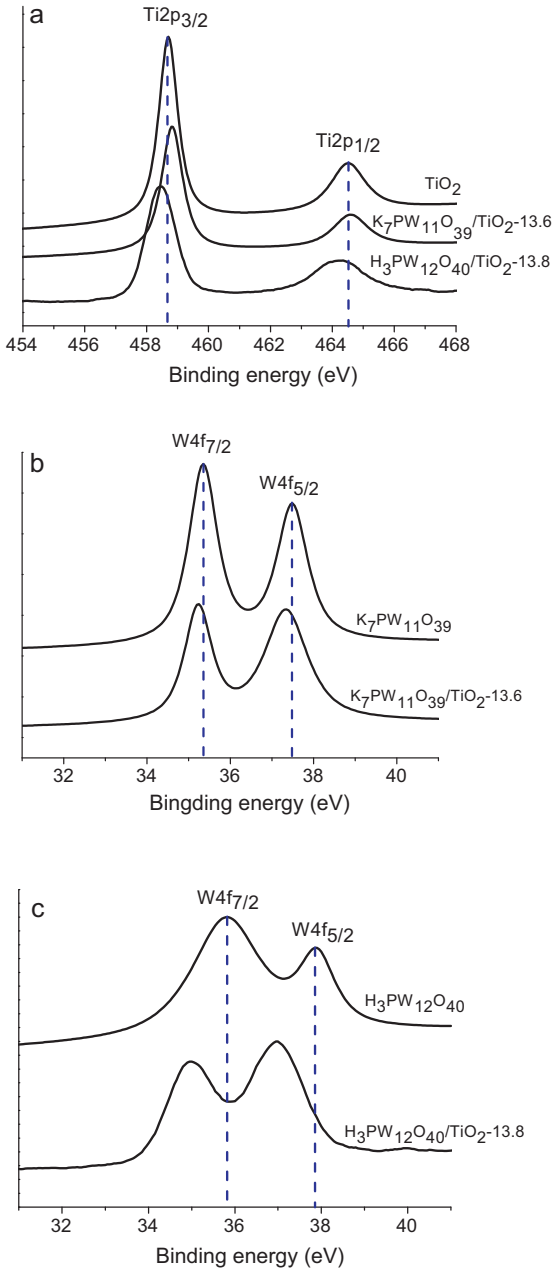

Fig. 1. XPS spectra of the starting $K_7PW_{11}O_{39}$ and $H_3PW_{12}O_{40}$ as well as TiO_2 materials with or without the incorporation of the Keggin unit in the Ti2p (a) and W4f (b and c) binding energy regions.

(Fig. 1). Fig. 1a displays high-resolution XP spectra of the tested samples in the $Ti2p_{3/2}$ and $Ti2p_{1/2}$ binding energy regions. The determined binding energies of $Ti2p_{3/2}$ and $Ti2p_{1/2}$ are 458.7 eV and 464.5 eV, respectively, characteristic of the Ti (IV) oxidation state in the Ti—O—Ti bonds of bulk TiO_2 [20]. After introduction of the Keggin unit into the TiO_2 framework, the binding energies of $Ti2p_{3/2}$ and $Ti2p_{1/2}$ have some shifts. For the $K_7PW_{11}O_{39}/TiO_2$ composite, the binding energies of $Ti2p_{3/2}$ and $Ti2p_{1/2}$ shift to higher values (458.8 eV and 464.6 eV). As for the $H_3PW_{12}O_{40}/TiO_2$, the corresponding binding energies shift to lower values (458.4 eV and 464.2 eV). The above result indicates that (1) a slight perturbation of titanium environment occurred due to the introduction of the Keggin unit, regardless of the saturated or lacunary structure; and (2) the interaction between TiO_2 framework and saturated or lacunary Keggin unit at the surface of the composite is different. The

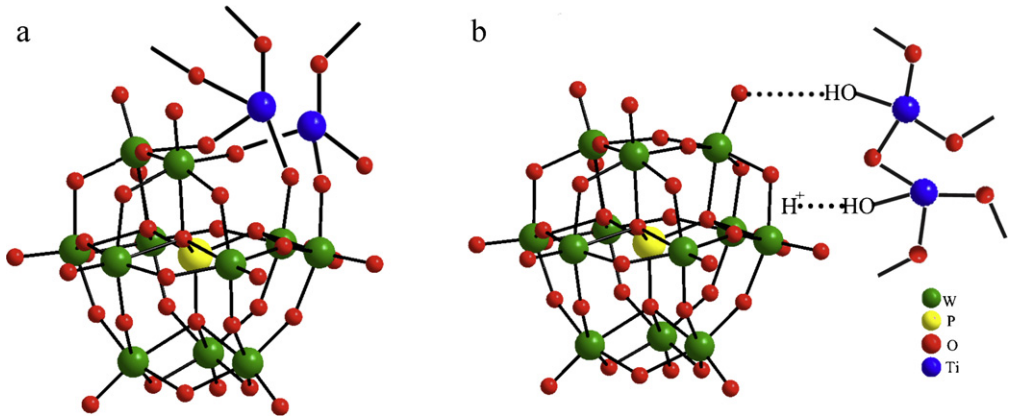

Scheme 1. The proposed framework structures of the $K_7PW_{11}O_{39}/TiO_2$ (a) and $H_3PW_{12}O_{40}/TiO_2$ (b) composite materials.

above interaction also results in some shifts of the binding energies of $W4f_{7/2}$ and $W4f_{5/2}$ for the $K_7PW_{11}O_{39}/TiO_2$ or $H_3PW_{12}O_{40}/TiO_2$ composite compared with those of the starting $K_7PW_{11}O_{39}$ or $H_3PW_{12}O_{40}$ unit. From the results displayed in Fig. 1b and c it is found that (1) the binding energies of $W4f_{7/2}$ and $W4f_{5/2}$ shift to lower values for both $K_7PW_{11}O_{39}/TiO_2$ and $H_3PW_{12}O_{40}/TiO_2$ composites compared with the starting $K_7PW_{11}O_{39}$ and $H_3PW_{12}O_{40}$; and (2) this shift is more obvious for the $H_3PW_{12}O_{40}/TiO_2$ compared with the $K_7PW_{11}O_{39}/TiO_2$ (the binding energies of $W4f_{7/2}$ and $W4f_{5/2}$ are 35.4 eV and 37.5 eV for $K_7PW_{11}O_{39}$; 35.8 eV and 37.8 eV for $H_3PW_{12}O_{40}$; 35.3 eV and 37.3 eV for $K_7PW_{11}O_{39}/TiO_2$-13.6; and 34.9 eV and 36.9 eV for $H_3PW_{12}O_{40}/TiO_2$-13.8 [21]).

XRD patterns (Fig. S2 of Supplementary Information) indicate that all tested $K_7PW_{11}O_{39}/TiO_2$ and $H_3PW_{12}O_{40}/TiO_2$ composites possess anatase phase structure with the characteristic 2θ values of 25.3° (101), 37.8° (103, 004, and 112), 48.1° (200), 54.4° (105, 211), 62.7° (204), 68.8° (116), 70.3° (220), 75.3° (215), and 82.5° (303), respectively (JCPDS NO. 21-1272). Additionally, the diffractions related to the Keggin unit are not found, implying homogeneous dispersion of the Keggin unit throughout the TiO_2 framework.

Based on the above FT-IR, XPS, and XRD results we conclude that the primary Keggin structure of the saturated or lacunary POM remained intact after being introduced into TiO_2 framework by current preparation route. Additionally, different kinds of the interactions existed between the saturated or lacunary Keggin unit and TiO_2 framework at the interface of the two components. Considering the structure characteristics of $K_7PW_{11}O_{39}$ and $H_3PW_{12}O_{40}$ together with well-matched electronegativity and ionic radius of Ti^{4+} ion (1.54, 0.0605 nm) and W^{6+} ion (1.70, 0.060 nm), these interactions are tentatively inferred. For the $H_3PW_{12}O_{40}/TiO_2$ composite, the saturated Keggin unit links with the TiO_2 framework through hydrogen bonding and acid–base interactions. On the one hand, the hydrogen bonds were formed in the $H_3PW_{12}O_{40}/TiO_2$ composite between the oxygen atoms of the Keggin unit and the surface hydroxyl groups of ≡Ti—OH groups of anatase TiO_2, which can be expressed in the forms of $W{=}O_d\cdots HO-Ti$, $W{-}O_c\cdots HO{-}Ti$, and $W{-}O_e\cdots HO{-}Ti$, where O_d and O_c/O_e refer to the terminal oxygen atoms and the bridge oxygen atoms of $H_3PW_{12}O_{40}$, respectively. On the other hand, chemically active surface ≡Ti—OH groups were protonated in an acidic medium to form the $\equiv Ti{-}OH_2^+$ groups. The $\equiv Ti{-}OH_2^+$ group should act as a counter ion for $H_3PW_{12}O_{40}$ and led to the $(\equiv Ti{-}OH_2^+)$ $(H_2PW_{12}O_{40}^-)$ species by acid–base reaction. In the case of $K_7PW_{11}O_{39}/TiO_2$, the starting $K_7PW_{11}O_{39}$ is the monovacant derivative of the $H_3PW_{12}O_{40}$, and the removal of a tungsten–oxygen octahedral from a saturated $PW_{12}O_{40}^{3-}$ framework leads to increase and localization of the anionic charge [22,23]. Accordingly, the resulting lacunary anion $(PW_{11}O_{39}^{7-})$ becomes highly nucleophilic and reacts easily with electrophilic groups. Additionally, hydrolysis and condensation of TTIP under acidic condition can yield $(OH)_{4-n}Ti(OTi)_n$ $(n = 1–4)$ species that construct the titania framework, and the framework has the electrophilic surface titanium atoms in surface ≡Ti—OH groups, which demonstrate chemical reactivity toward monovacant $K_7PW_{11}O_{39}$. Therefore, the $K_7PW_{11}O_{39}/TiO_2$ composite was formed through grafting of two ≡Ti—OH groups to the surface of $K_7PW_{11}O_{39}$. In this kind of the $K_7PW_{11}O_{39}/TiO_2$ composite, $K_7PW_{11}O_{39}$ presents one vacant site, which allows connecting two TiO_4 units of the titania network to make up one tungsten–oxygen octahedral lacuna. Therefore, the terminal nuclephilic oxygen atoms of the $K_7PW_{11}O_{39}$ become bridge atoms due to connecting with the electrophilic titanium atoms in ≡Ti—OH groups *via* W—O—Ti bridge bonds. According to the above discussion the proposed framework structures of the $K_7PW_{11}O_{39}/TiO_2$ and $H_3PW_{12}O_{40}/TiO_2$ composite materials are displayed in Scheme 1.

3.1.2. Optical absorption properties

The optical absorption properties that are relevant to the electronic structure feature of the photocatalytic materials are recognized as the key factors in determining their photocatalytic activity. Herein, the optical absorption properties of as-prepared $K_7PW_{11}O_{39}/TiO_2$ and $H_3PW_{12}O_{40}/TiO_2$ were investigated by UV–Vis/DRS; for comparison, the starting $K_7PW_{11}O_{39}$ and $H_3PW_{12}O_{40}$ as well as pure TiO_2 were also tested (Fig. 2). The result shows each TiO_2-based material has a steep and parallel absorption band starting from 200 nm and ending up to *ca.*

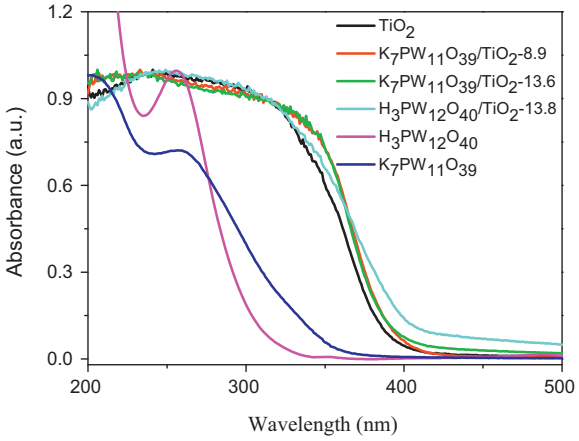

Fig. 2. UV–Vis/DRS of the starting $K_7PW_{11}O_{39}$ and $H_3PW_{12}O_{40}$, pure TiO_2 as well as the supported $K_7PW_{11}O_{39}/TiO_2$ and $H_3PW_{12}O_{40}/TiO_2$-13.8 materials.

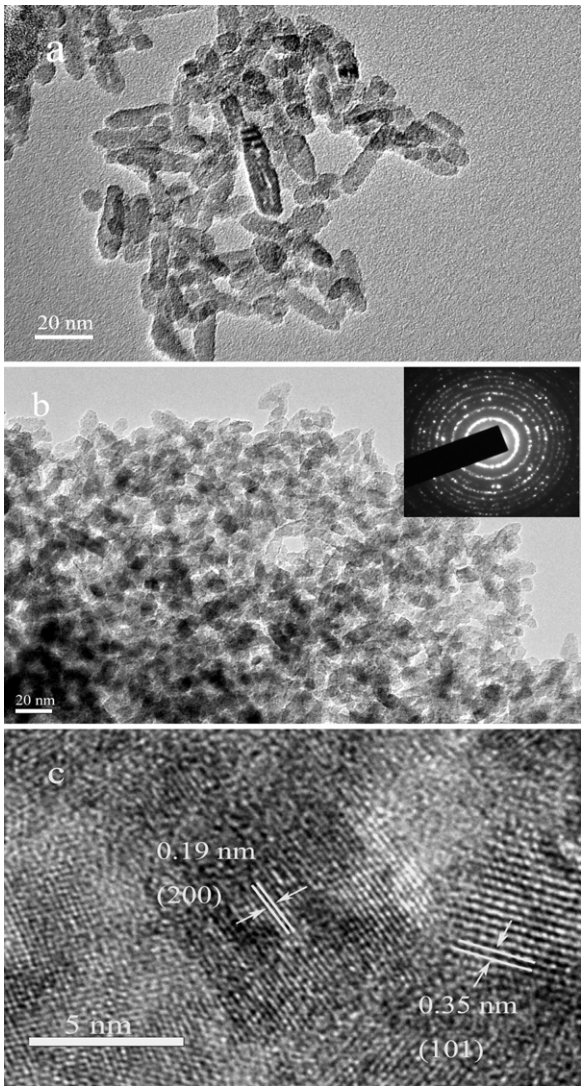

Fig. 3. TEM images of TiO_2 (a) and $K_7PW_{11}O_{39}/TiO_2$-13.6 (b). HRTEM image of $K_7PW_{11}O_{39}/TiO_2$-13.6 (c).

400 nm. Additionally, compared with pure TiO_2, the absorption band of $K_7PW_{11}O_{39}/TiO_2$ and $H_3PW_{12}O_{40}/TiO_2$ has a slight red-shift, and the separated absorption peak corresponding to either $K_7PW_{11}O_{39}$ or $H_3PW_{12}O_{40}$ (*ca.* 260 nm) was not found. The result suggests the presence of Keggin unit has an influence on the electronic properties of anatase TiO_2. For pure TiO_2, the absorption band is originated from the charge transfer from O2p orbital to Ti3d orbital, while for the starting $K_7PW_{11}O_{39}$ and $H_3PW_{12}O_{40}$, the band is assigned to the charge transfer from O2p orbital to W5d orbital. In the cases of $K_7PW_{11}O_{39}/TiO_2$ and $H_3PW_{12}O_{40}/TiO_2$, the absorption band corresponds to the charge transfer from O2p orbital to the new conduction band of the composites. This new conduction band is constructed from the hybridization of Ti3d orbital and W5d orbital since they possess similar energy levels [11,13].

3.1.3. Morphology and textural properties

The representative TEM observations reveal the prepared pure TiO_2 and $K_7PW_{11}O_{39}/TiO_2$ composite are sphere-shaped with a size of *ca.* 10 nm (Fig. 3a and b), and aggregation among the particles is observed. Moreover, the nanocrystalline nature of the composite can be visibly observed in its HRTEM image (Fig. 3c). The lattice fringe that is used for phase determination is 0.35 nm and 0.19 nm, corresponding to the lattice spacing of (1 0 1) and (2 0 0) plane of the

Table 2
Textural parameters of pure TiO_2, $K_7PW_{11}O_{39}/TiO_2$, and $H_3PW_{12}O_{40}/TiO_2$-13.8 materials.

Sample	S_{BET} ($m^2\,g^{-1}$)[a]	V_p ($cm^3\,g^{-1}$)[b]	D_p (nm)[c]
TiO_2	164	0.35	7.9
$K_7PW_{11}O_{39}/TiO_2$-8.9	151	0.38	8.4
$K_7PW_{11}O_{39}/TiO_2$-13.6	154	0.41	10.8
$H_3PW_{12}O_{40}/TiO_2$-13.8	168	0.28	6.6

[a] S_{BET} (BET surface area) was estimated from the BET equation.
[b] V_p (pore volume) was estimated from the pore volume determined using the adsorption branch of the nitrogen isotherm curve at $P/P_0 = 0.97$ single point.
[c] D_p (median pore diameter) was estimated by using BJH model based on nitrogen desorption isotherm.

$K_7PW_{11}O_{39}/TiO_2$. The SAED pattern further confirms the anatase structure of $K_7PW_{11}O_{39}/TiO_2$ material, and the rings from the inner to the outer correspond to (1 0 1), (0 0 4), (2 0 0), (1 0 5/2 1 1), and (2 0 4) diffraction of anatase phase, respectively (inset in Fig. 3b).

All tested materials including pure TiO_2, $K_7PW_{11}O_{39}/TiO_2$, and $H_3PW_{12}O_{40}/TiO_2$ exhibit a type IV adsorption isotherm with a H3 hysteresis loop, which are typical characteristics of mesoporous materials with a larger pore diameter formed by aggregation of the primary nanocrystallites (Fig. S3 of Supplementary Information). The BET surface areas of $K_7PW_{11}O_{39}/TiO_2$ composites decrease from 164 $m^2\,g^{-1}$ to 151 $m^2\,g^{-1}$ with the increase of $K_7PW_{11}O_{39}$ loading from 0% to 13.6% (Table 2). Additionally, the calculated pore diameter based on BJH model of nitrogen desorption isotherm of the $K_7PW_{11}O_{39}/TiO_2$ and $H_3PW_{12}O_{40}/TiO_2$ is higher and lower than that of pure TiO_2, respectively.

3.2. Photocatalytic tests

The simulated sunlight (320 nm < λ < 680 nm) photocatalytic activity of the $K_7PW_{11}O_{39}/TiO_2$ and $H_3PW_{12}O_{40}/TiO_2$ as well as pure TiO_2 was evaluated and compared by the degradation of two target compounds including dye RB (25 mg L^{-1}, 100 mL) and endocrine-disrupting chemical DEP (20 mg L^{-1}, 100 mL). At the same time, the interactions between RB (DEP) molecule and $K_7PW_{11}O_{39}/TiO_2$ or $H_3PW_{12}O_{40}/TiO_2$ composite were studied before the photocatalytic tests. It is reported that this interaction is indispensable for the efficient photoinduced electron injection and the subsequent degradation reactions, and that both the surface properties of the photocatalyst particles and the structures of the target pollutants can exert great effect on this interaction [24].

3.2.1. Adsorption and photocatalytic degradation of RB

The interaction between RB molecule and TiO_2 or POM/TiO_2 particles was studied firstly. From the result shown in Fig. 4a it is observed that after stirring the suspension of the catalyst and RB solution for 30 min in the dark, disappearance of RB reaches to 5.3% (TiO_2), 17.5% ($K_7PW_{11}O_{39}/TiO_2$-8.9), 30.9% ($K_7PW_{11}O_{39}/TiO_2$-13.6), and 34.6% ($H_3PW_{12}O_{40}/TiO_2$-13.8), respectively; and RB concentration remains unchangeable with further increasing the stirring time to 60 min. The result indicates adsorption–desorption equilibrium between RB molecules and the catalyst is established after 30 min stirring. Difference of the adsorption capacity for the above TiO_2-based photocatalysts is explained as follows. RB molecule is known to be bound on the TiO_2 surface *via* esterification between its carboxylic group and the surface hydroxyl group of TiO_2 [24]. In the case of the $K_7PW_{11}O_{39}/TiO_2$, nucleophilic monovacant $PW_{11}O_{39}^{7-}$ strongly interacts with the positively charged diethylamine group of RB; meanwhile, esterification between RB and TiO_2 surface also exists. Accordingly, the adsorption capacity of the $K_7PW_{11}O_{39}/TiO_2$ is higher than that of pure TiO_2; moreover, higher $K_7PW_{11}O_{39}$ loading results in higher absorption capacity of the $K_7PW_{11}O_{39}/TiO_2$ towards RB

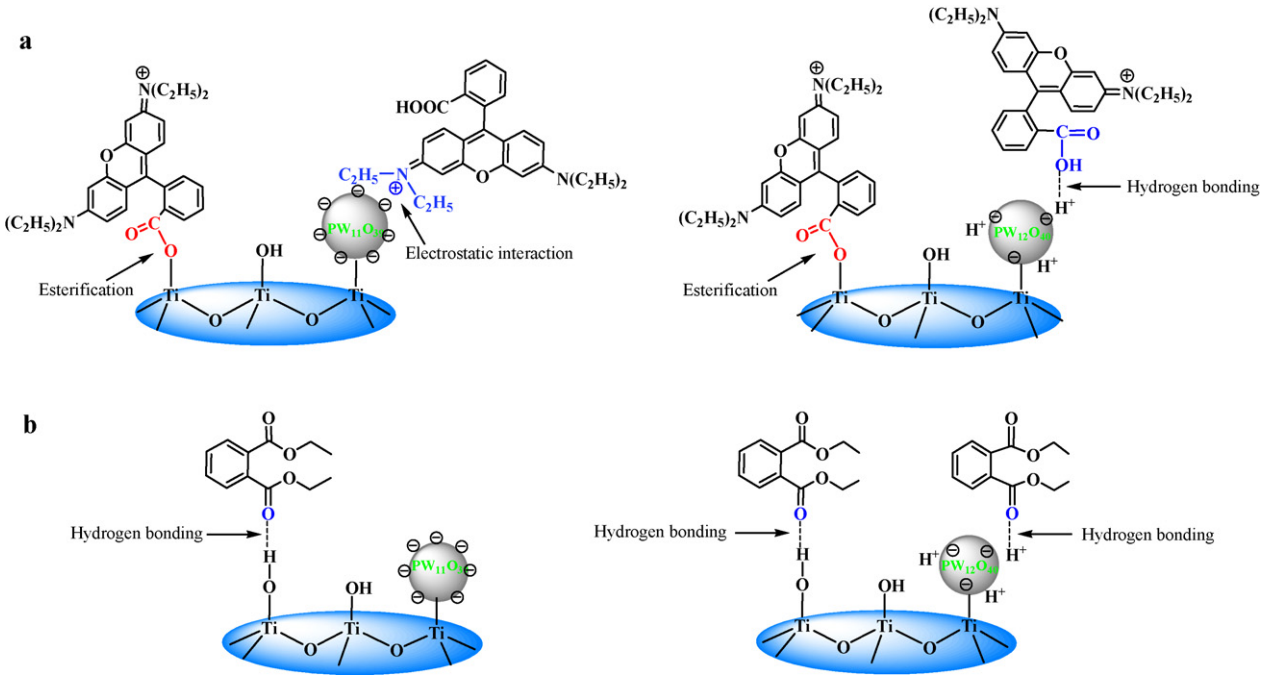

Scheme 2. Adsorption modes of RB (a) and DEP (b) in aqueous $K_7PW_{11}O_{39}/TiO_2$ (left) and $H_3PW_{12}O_{40}/TiO_2$ (right) dispersions.

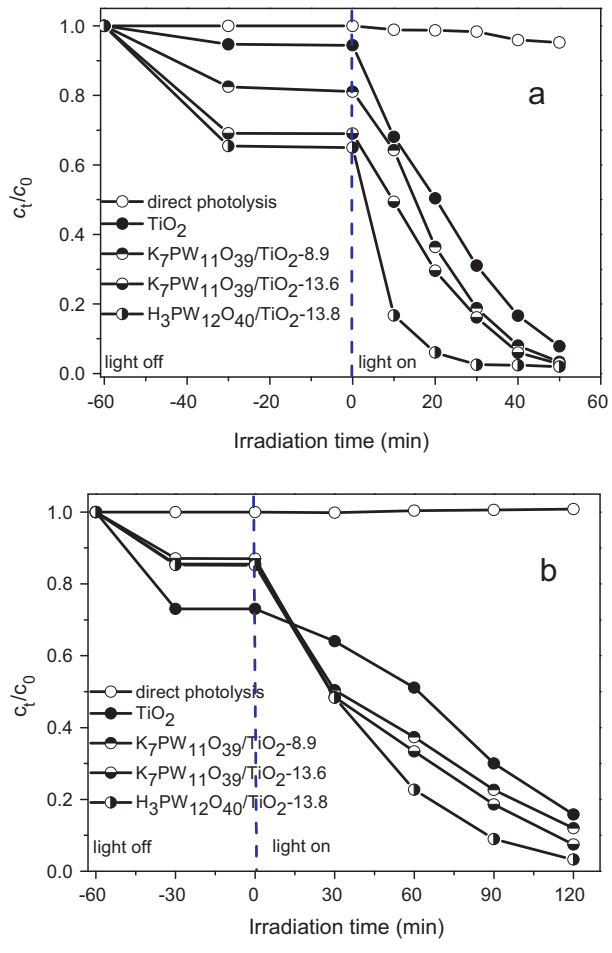

Fig. 4. Photocatalytic degradation of RB (a) and DEP (b) under simulated sunlight irradiation of TiO_2, $K_7PW_{11}O_{39}/TiO_2$, and $H_3PW_{12}O_{40}/TiO_2$-13.8 materials. c_0 and c_t is the original and residual RB or DEP concentration in the reaction system. c_0^{RB} = 25 mg L^{-1} and c_0^{DEP} = 20 mg L^{-1}; volume: 100 mL; catalyst: 150 mg.

owing to the enhanced interaction between $PW_{11}O_{39}^{7-}$ cluster and the positively charged diethylamine group of RB. Similarly, both esterification and hydrogen bonding (formed *via* the interaction of hydroxyl group of RB and protons of $H_3PW_{12}O_{40}$) existed between the $H_3PW_{12}O_{40}/TiO_2$ composite and RB molecule. Additionally, the $H_3PW_{12}O_{40}/TiO_2$ composite possesses the largest BET surface area among all tested TiO_2-based materials, which may also contribute to its strong adsorption ability. Based on the above discussion, the proposed adsorption modes of RB in aqueous $K_7PW_{11}O_{39}/TiO_2$ and $H_3PW_{12}O_{40}/TiO_2$ dispersions are illustrated in Scheme 2a.

The photocatalytic test displayed in Fig. 4a indicates that the initial RB concentration is almost unchangeable under the solar simulating Xe lamp irradiation for 50 min. However, significant degradation of RB occurs in the presence of both the simulated sunlight irradiation and photocatalyst, and conversion of RB reaches to 83.4% (TiO_2), 92.0% ($K_7PW_{11}O_{39}/TiO_2$-8.9), 94.0% ($K_7PW_{11}O_{39}/TiO_2$-13.6), and 97.6% ($H_3PW_{12}O_{40}/TiO_2$-13.8), respectively, under the simulated sunlight irradiation for 40 min.

3.2.2. Adsorption and photocatalytic degradation of DEP

The photocatalytic activity of the $K_7PW_{11}O_{39}/TiO_2$ and $H_3PW_{12}O_{40}/TiO_2$ was further examined by a light insensitive target compound DEP. DEP is a typical endocrine-disrupting chemical that has a wide variety of industrial, agricultural, and domestic applications, especially for their uses as plasticizers. DEP is rather stable in the natural environment, and it recalcitrates to biodegradation and photolytic degradation owing to the existence of benzene carboxylic group and lack of light response at wavelengths longer than 300 nm [25,26]. Thus, elimination of DEP from water is very important.

The adsorption tests show that the adsorption behavior of the tested TiO_2-based catalysts to DEP molecule is different from RB, which originates from the different structures of the model molecules selected. As depicted in Fig. 4b, the adsorption–desorption between the DEP molecule and the tested catalysts reaches equilibrium after 30 min stirring before light on. Additionally, the adsorption capacity of TiO_2 is higher than that of the $K_7PW_{11}O_{39}/TiO_2$ or $H_3PW_{12}O_{40}/TiO_2$. For example, after

stirring the suspension of the catalyst and DEP solution for 30 min before light on, disappearance of DEP reaches to 26.9% (TiO_2), 14.5% ($K_7PW_{11}O_{39}/TiO_2$-8.9), 12.9% ($K_7PW_{11}O_{39}/TiO_2$-13.6), and 14.8% ($H_3PW_{12}O_{40}/TiO_2$-13.8), respectively. Adsorption of DEP molecules on the TiO_2 surface is due to the hydrogen bonding existed between the surface hydroxyl groups of TiO_2 and the most negative oxygen atoms (*i.e.* two carbonyl oxygen atoms) of DEP molecules [27]. After the incorporation of the Keggin unit into TiO_2 framework, considerable amount of surface hydroxyl groups of TiO_2 lost due to the interaction of the Keggin unit with TiO_2 framework. As a consequence, the adsorption ability of the $K_7PW_{11}O_{39}/TiO_2$ or $H_3PW_{12}O_{40}/TiO_2$ becomes weaker compared with pure TiO_2. Accordingly, higher $K_7PW_{11}O_{39}$ loading results in the lower adsorption capacity. The proposed adsorption modes of DEP in aqueous $K_7PW_{11}O_{39}/TiO_2$ and $H_3PW_{12}O_{40}/TiO_2$ dispersions are illustrated in Scheme 2b.

Degradation of DEP by direct photolysis is hardly observed after solar simulating Xe lamp irradiation for 120 min. However, significant degradation of DEP occurs in the presence of both the simulated sunlight irradiation and photocatalyst, and the conversion of DEP reaches to 84.2%, 88.0%, 92.6%, and 96.7%, respectively, after the simulating Xe lamp irradiation of TiO_2, $K_7PW_{11}O_{39}/TiO_2$-8.9, $K_7PW_{11}O_{39}/TiO_2$-13.6, and $H_3PW_{12}O_{40}/TiO_2$-13.8 for 120 min. The above tests show that as-prepared $K_7PW_{11}O_{39}/TiO_2$ and $H_3PW_{12}O_{40}/TiO_2$ composites also exhibit considerably higher simulated sunlight photocatalytic activity than pure TiO_2 towards light insensitive target compound DEP.

3.2.3. Mineralization of RB and DEP

The mineralization ability of the photocatalyst towards the target pollutant is an important standard to evaluate its photocatalytic activity. Herein, the mineralization ability of the $K_7PW_{11}O_{39}/TiO_2$-13.6 and $H_3PW_{12}O_{40}/TiO_2$-13.8 towards RB and DEP was evaluated by monitoring the changes of TOC in the reaction systems. For comparison, TiO_2 was also tested under the same conditions. From the results illustrated in Fig. 5a it is observed that the mineralization ability of the tested materials to RB follows the order $H_3PW_{12}O_{40}/TiO_2$-13.8 > $K_7PW_{11}O_{39}/TiO_2$-13.6 > TiO_2. After the simulated sunlight irradiation of RB and the catalyst for 10 h, the disappearance of TOC in the related reaction system reaches to 80.7% ($H_3PW_{12}O_{40}/TiO_2$-13.8), 73.6% ($K_7PW_{11}O_{39}/TiO_2$-13.6), and 67.5% (TiO_2), respectively. Similar result also can be observed for the mineralization of DEP, and the disappearance of TOC in $K_7PW_{11}O_{39}/TiO_2$-13.6- and $H_3PW_{12}O_{40}/TiO_2$-13.8-catalyzed DEP degradation system reaches to 82.6% and 87.6%, respectively, after the simulated sunlight irradiation of DEP for 10 h (Fig. 5b). The results indicate as-prepared $H_3PW_{12}O_{40}/TiO_2$ and $K_7PW_{11}O_{39}/TiO_2$ composites also exhibit mineralization ability towards aqueous RB and DEP.

The above photocatalytic tests indicate that (1) at the same POM loading, the saturated Keggin unit functionalized $H_3PW_{12}O_{40}/TiO_2$ composite material shows higher simulated sunlight photocatalytic activity in comparison to the monovacant Keggin unit functionalized $K_7PW_{11}O_{39}/TiO_2$; and (2) both $K_7PW_{11}O_{39}/TiO_2$ and $H_3PW_{12}O_{40}/TiO_2$ exhibit higher photoactivity than that of pure TiO_2. These results are explained based on the active species identified during DEP photodegradation and the changes of photocurrent responses in different photocatalytic systems.

3.2.4. Free radical and hole scavenging experiments

Generally, the photocatalytic degradation of organic pollutants by the semiconductor-based materials is controlled by active species including free radical species and holes. During the process of the photoexcitation of the photocatalytic materials, various kinds of active species like $O_2^{\bullet -}$, $^{\bullet}OOH$, $HO^{\bullet}$, and h_{VB}^+ can produce [28–31]. Herein, the target active species yielded in the

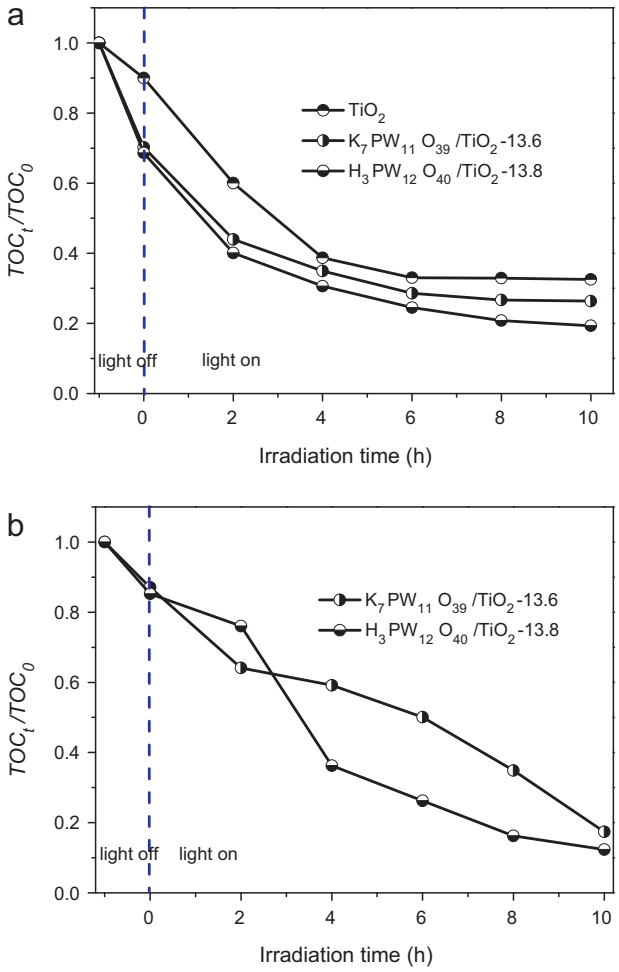

Fig. 5. Changes of TOC in the reaction systems during the process of the simulated sunlight photocatalytic degradation of RB (a) and DEP (b) over various catalysts. TOC_0 and TOC_t is the original and residual RB or DEP total organic carbon in the reaction system. $c_0^{RB} = 25$ mg L^{-1} and $c_0^{DEP} = 20$ mg L^{-1}; volume: 100 mL; catalyst: 150 mg.

$K_7PW_{11}O_{39}/TiO_2$- and $H_3PW_{12}O_{40}/TiO_2$-catalyzed DEP degradation systems were analyzed according to their influence on the reaction rate of the DEP degradation reaction by the free radical and hole scavenging experiments. As shown in Fig. 6, under the simulated sunlight irradiation of the $K_7PW_{11}O_{39}/TiO_2$ or $H_3PW_{12}O_{40}/TiO_2$, the photodegradation rate of DEP is markedly suppressed by the addition of hole scavenger (EDTA) and hydroxyl radical scavenger (t-BuOH). Similarly, the superoxide radical trapping experiment shows that the photodegradation of DEP becomes slow after the addition of 1,4-benzoquinone (BQ, superoxide radical scavenger) in both of the systems [32]. From the fact that DEP degradation catalyzed by the $K_7PW_{11}O_{39}/TiO_2$ or $H_3PW_{12}O_{40}/TiO_2$ is obviously suppressed by the addition of methanol it is inferred that the $^{\bullet}OOH$ species does not serve as the active species that is responsible for DEP degradation in current systems since the degradation rate of DEP would be greatly accelerated by methanol if $^{\bullet}OOH$ is an effective oxidant [33].

$$POM/TiO_2 \xrightarrow[320\,nm<\lambda<680\,nm]{\text{simulated sunlight}} POM/TiO_2\,(h_{VB}^+ + e_{CB}^-) \quad (1)$$

$$h_{VB}^+ + H_2O \rightarrow HO^{\bullet} + H^+ \quad (2)$$

$$O_2 + 2H_2O + 2e_{CB}^- \rightarrow H_2O_2 + 2OH^- \quad (3)$$

$$H_2O_2 + e_{CB}^- \rightarrow HO^{\bullet} + H^- \quad (4)$$

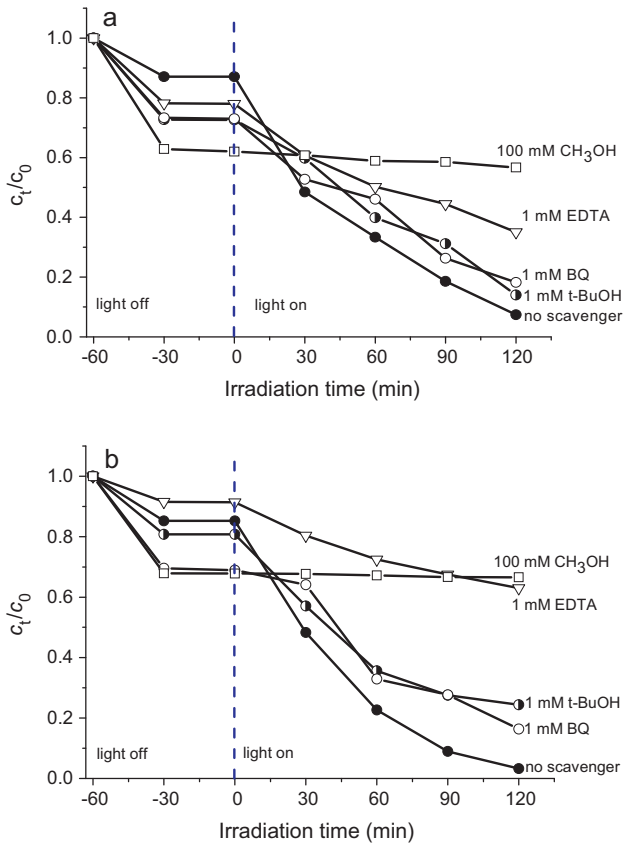

Fig. 6. Plots of photogenerated carrier scavenging in the system of photodegradation of DEP on $K_7PW_{11}O_{39}/TiO_2$-13.6 (a) and $H_3PW_{12}O_{40}/TiO_2$-13.8 (b). $c_0 = 20\,mg\,L^{-1}$; volume: 100 mL; catalyst: 150 mg.

$$POM + e_{CB}^- \rightarrow POM^- \quad (5)$$

$$POM^- + O_2 \rightarrow POM + O_2^{\bullet -} \quad (6)$$

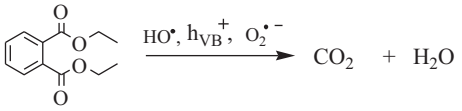

(7)

The above results indicate that the active species including HO•, h_{VB}^+, and $O_2^{\bullet -}$ are responsible for the degradation of DEP in current simulated sunlight irradiated POM/TiO_2 systems. Under the simulated sunlight irradiation of the band gap of the POM/TiO_2, the photogenerated e_{CB}^- and h_{VB}^+ are generated (Eq. (1)). The h_{VB}^+ subsequent transfers into HO• radicals by the oxidation of OH^- or the reduction of dioxygen dissolved in aqueous solution (Eqs. (2)–(4)). In addition, the e_{CB}^- can easily transfer into the W5d empty orbits of $K_7PW_{11}O_{39}$ or $H_3PW_{12}O_{40}$ unit and thereby realizing the effective separation of the h_{VB}^+–e_{CB}^- pairs (Eq. (5)). The reduced form of POM^- can be easily reoxidized by dioxygen and returns to its oxidized form accompanying with the production of $O_2^{\bullet -}$ radicals (Eq. (6)). With the help of HO•, h_{VB}^+, and $O_2^{\bullet -}$ species, DEP is degraded and then mineralized into CO_2 and H_2O (Eq. (7)).

3.2.5. Photocurrent investigation

It is reported that the photocatalytic activity of the photocatalyst mainly depends on the photoelectron generation, h_{VB}^+–e_{CB}^- pair separation, and the electron-transfer efficiency on the photocatalyst surface [34]. In current UV-light irradiating TiO_2/Ti or POM/TiO_2/Ti system, the photoelectrochemical experiments were carried out for the purposes of (1) investigation of the interfacial

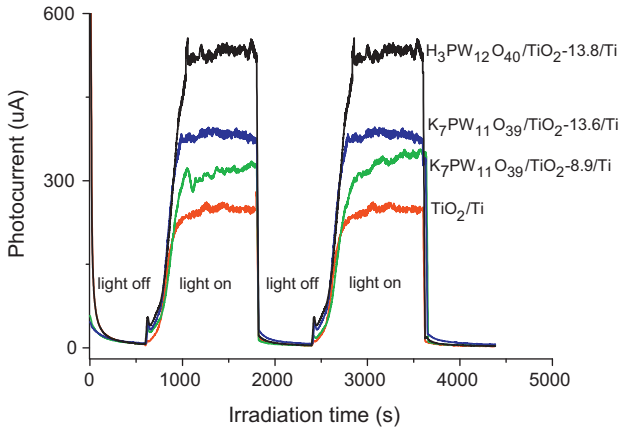

Fig. 7. Photocurrent responses of TiO_2/Ti, $K_7PW_{11}O_{39}/TiO_2$/Ti, and $H_3PW_{12}O_{40}/TiO_2$-13.8/Ti electrodes in 0.01 M Na_2SO_4 electrolyte solution under UV illumination (the working electrode potential was constant at +1.0 V).

electron-transfer process of TiO_2 or POM/TiO_2 and thereby understanding the synergistic photocatalytic effect between the Keggin unit and TiO_2, which may provide powerful evidence to explain the higher photocatalytic activity of the POM/TiO_2 than that of pure TiO_2; and (2) explanation of the activity difference between $H_3PW_{12}O_{40}/TiO_2$ and $K_7PW_{11}O_{39}/TiO_2$.

From photocurrent–time (I–t) profiles shown in Fig. 7 it can be seen that (1) the sharp increased photocurrent responses appear for all tested TiO_2/Ti-based electrodes once the pulse UV-light irradiation was applied; (2) the produced photocurrents are reproducible and stable during several light on/off cycles; (3) the $H_3PW_{12}O_{40}/TiO_2$/Ti electrode and the TiO_2/Ti electrode exhibits the highest and the lowest photocurrent response, respectively, under the same testing conditions; and (4) for the two tested $K_7PW_{11}O_{39}/TiO_2$/Ti electrodes with $K_7PW_{11}O_{39}$ loading of 8.9% and 13.6%, higher $K_7PW_{11}O_{39}$ loading (13.6%) results in higher photocurrent response of $K_7PW_{11}O_{39}/TiO_2$/Ti electrode. The prompt increase in photocurrent response from the light-off to light-on state is mainly ascribed to the fast transfer of the photogenerated e_{CB}^- on the surface of the TiO_2/Ti-based electrodes. Accordingly, it is inferred that the transfer of the photogenerated e_{CB}^- on the surface of the $H_3PW_{12}O_{40}/TiO_2$/Ti electrode is faster than that of the $K_7PW_{11}O_{39}/TiO_2$/Ti electrode (under the same POM loading); additionally, the Keggin unit functionalized POM/TiO_2/Ti electrodes, regardless of the saturated or lacunary structure, show more rapid photogenerated e_{CB}^- transfer ability compared to TiO_2/Ti electrodes.

The above result is reasonably explained based on the structure characteristic of the saturated and lacunary Keggin unit. Higher photocurrent response of $H_3PW_{12}O_{40}/TiO_2$/Ti or $K_7PW_{11}O_{39}/TiO_2$/Ti electrode compared with TiO_2/Ti electrode is due to the superior electron accepting ability of the polyoxotungstates. It is more feasible to facilitate the charge transfer mediated by polyoxotungstates than direct transfer from the TiO_2 conductor band to the connection electrode [34]. This is the well-known synergistic photocatalytic effect existed between the Keggin unit and TiO_2. In addition, compared with $K_7PW_{11}O_{39}$, $H_3PW_{12}O_{40}$ has more unoccupied W5d orbits and is easier to accept the photogenerated e_{CB}^- from the TiO_2 conductor band. Therefore, a higher photocurrent response or a lower h_{VB}^+–e_{CB}^- pair recombination probability can be realized, resulting in higher photoelectron-conversion efficiency for the $H_3PW_{12}O_{40}/TiO_2$/Ti photoanode with respect to $K_7PW_{11}O_{39}/TiO_2$/Ti photoanode. Eventually, the enhanced photocatalytic activity of the $H_3PW_{12}O_{40}/TiO_2$ with respect to $K_7PW_{11}O_{39}/TiO_2$ was obtained.

3.2.6. Recyclability of the catalyst

The stability and reusability of the catalysts are very important issue for their practical applications. Herein, $K_7PW_{11}O_{39}/TiO_2$-13.6 and $H_3PW_{12}O_{40}/TiO_2$-13.8 were chosen to evaluate the recyclability of the photocatalysts by four times' RB degradation reaction. After the first catalytic run, the photocatalyst separated from the reaction mixture by centrifugation was washed with doubly distilled water one time and ethanol three times to remove the absorbed RB and intermediates. Subsequently, the catalyst was dried at 353 K for 12 h. The recovered catalyst was used for subsequent catalytic runs under the same experimental conditions. After four catalytic runs the photocatalytic activity loss was hardly observed in both $K_7PW_{11}O_{39}/TiO_2$-13.6- and $H_3PW_{12}O_{40}/TiO_2$-13.8-catalyzed RB degradation systems (Fig. S4 of Supplementary Information); meanwhile, P or W was hardly detected by ICP-AES in the catalyst-free reaction solutions. The results confirm as-prepared $K_7PW_{11}O_{39}/TiO_2$ and $H_3PW_{12}O_{40}/TiO_2$ composite materials are of considerably catalytic stability, which is due to the chemical rather than physical interaction existed between the Keggin unit and TiO_2 support.

4. Conclusions

One-step prepared $K_7PW_{11}O_{39}/TiO_2$ and $H_3PW_{12}O_{40}/TiO_2$ composite materials exhibited higher simulated sunlight photocatalytic activity towards the degradation and mineralization of dye RB and endocrine-disrupting chemical DEP than pure TiO_2; and at the same POM loading, $H_3PW_{12}O_{40}/TiO_2$ was more photoactive than that of $K_7PW_{11}O_{39}/TiO_2$. The excellent photocatalytic performance of as-prepared POM/TiO_2 composite materials with respect to pure TiO_2 is mainly attributed to the synergistic photocatalytic effect confirmed by the photoelectrochemical experiment, which results in a lower h_{VB}^+–e_{CB}^- pair recombination probability. And the photocatalytic activity difference between the saturated and monovacant Keggin unit functionalized titania material is due to their structure difference, which resulted in their different electron-accepting ability. The free radical and hole scavenging experiments show that the active species including $HO^\bullet$, h_{VB}^+, and $O_2^{\bullet-}$ are responsible for the degradation and mineralization of the target compounds in current simulated sunlight irradiated POM/TiO_2 systems.

Acknowledgements

This work was supported by the Fundamental Research Funds for the Central Universities (09QNTD004), the Natural Science Fund Council of China (21173036 and 51008056), and the Science and Technology Project of Jilin Province (201101002).

Appendix A. Supplementary data

Supplementary data associated with this article can be found, in the online version, at doi:10.1016/j.colsurfa.2012.03.036.

References

[1] A. Fujishima, T.N. Rao, D.A. Tryk, Titanium dioxide photocatalysis, J. Photochem. Photobiol. C 1 (2000) 1–21.
[2] M.N. Chong, B. Jin, C.W.K. Chow, C. Saint, Recent developments in photocatalytic water treatment technology: a review, Water Res. 44 (2010) 2997–3027.
[3] C.G. Silva, R. Juárez, T. Marino, R. Molinari, H. García, Influence of excitation wavelength (UV or visible Light) on the photocatalytic activity of titania containing gold nanoparticles for the generation of hydrogen or oxygen from water, J. Am. Chem. Soc. 133 (2011) 595–602.
[4] X.B. Chen, S.S. Mao, Titanium dioxide nanomaterials: synthesis, properties, modifications, and applications, Chem. Rev. 107 (2007) 2891–2959.
[5] M.D. Hernández-Alonso, F. Fresno, S. Suárez, J.M. Coronado, Development of alternative photocatalysts to TiO_2: challenges and opportunities, Energy Environ. Sci. 2 (2009) 1231–1257.
[6] A. Hiskia, A. Mylonas, E. Papaconstantinou, Comparison of the photoredox properties of polyoxometallates and semiconducting particles, Chem. Soc. Rev. 30 (2001) 62–69.
[7] M. Misono, Unique acid catalysis of heteropoly compounds (heteropolyoxometalates) in the solid state, Chem. Commun. (2001) 1141–1152.
[8] P. Kormali, T. Triantis, D. Dimotikali, A. Hiskia, E. Papaconstantinou, On the photooxidative behavior of TiO_2 and $PW_{12}O_{40}^{3-}$: OH radicals versus holes, Appl. Catal. B: Environ. 68 (2006) 139–146.
[9] M.J. Yoon, J.A. Chang, Y. Kim, J.R. Choi, K. Kim, S.J. Lee, Heteropoly acid-incorporated TiO_2 colloids as novel photocatalytic systems resembling the photosynthetic reaction center, J. Phys. Chem. B 105 (2001) 2539–2545.
[10] R.R. Ozer, J.L. Ferry, Investigation of the photocatalytic activity of TiO_2–polyoxometalate systems, Environ. Sci. Technol. 35 (2001) 3242–3246.
[11] L. Li, Q.Y. Wu, Y.H. Guo, C.W. Hu, Nanosize and bimodal porous polyoxotungstate–anatase TiO_2 composites: preparation and photocatalytic degradation of organophosphorus pesticide using visible-light excitation, Micropor. Mesopor. Mater. 87 (2005) 1–9.
[12] Y. Yang, Q.Y. Wu, Y.H. Guo, C.W. Hu, E.B. Wang, Efficient degradation of dye pollutants on nanoporous polyoxotungstate–anatase composite under visible-light irradiation, J. Mol. Catal. A: Chem. 225 (2005) 203–212.
[13] K.X. Li, X. Yang, Y.N. Guo, F.Y. Ma, H.C. Li, L. Chen, Y.H. Guo, Design of mesostructured $H_3PW_{12}O_{40}$–titania materials with controllable structural orderings and pore geometries and their simulated sunlight photocatalytic activity towards diethyl phthalate degradation, Appl. Catal. B: Environ. 99 (2010) 364–375.
[14] G. Marcì, E. García-López, L. Palmisano, Photo-assisted degradation of 2-propanol in gas–solid regime by using TiO_2 impregnated with heteropolyacid $H_3PW_{12}O_{40}$, Catal. Today 144 (2009) 42–47.
[15] G. Marcì, E. García-López, L. Palmisano, D. Carriazo, C. Martín, V. Rives, Preparation, characterization and photocatalytic activity of TiO_2 impregnated with the heteropolyacid $H_3PW_{12}O_{40}$: photo-assisted degradation of 2-propanol in gas–solid regime, Appl. Catal. B: Environ. 90 (2009) 497–506.
[16] Y.H. Guo, Y.H. Wang, C.W. Hu, Y.H. Wang, E.B. Wang, Y.C. Zhou, S.H. Feng, Microporous polyoxometalates POMs/SiO_2: synthesis and photocatalytic degradation of aqueous organocholorine pesticides, Chem. Mater. 12 (2000) 3501–3508.
[17] C. Brevard, R. Schimpf, G. Tourne, C.M. Tourne, Tungsten-183 NMR: a complete and unequivocal assignment of the tungsten–tungsten connectivities in heteropolytungstates via two-dimensional ^{183}W NMR techniques, J. Am. Chem. Soc. 105 (1983) 7059–7063.
[18] N. Haraguchi, Y. Okaue, T. Isobe, Y. Matsuda, Stabilization of tetravalent cerium upon coordination of unsaturated heteropolytungstate anions, Inorg. Chem. 33 (1994) 1015–1020.
[19] P.A. Shringarpure, A. Patel, Liquid phase oxidation of styrene over zirconia supported undecatungstophosphate using different oxidants: a comparative study, Dalton Trans. 39 (2010) 2615–2621.
[20] H.W. Chen, Y. Ku, Y.L. Kuo, Effect of Pt/TiO_2 characteristics on temporal behavior of o-cresol decomposition by visible light-induced photocatalysis, Water Res. 41 (2007) 2069–2078.
[21] J.H. Li, W.L. Kang, X. Yang, X.D. Yu, L.L. Xu, Y.H. Guo, H.B. Fang, S.D. Zhang, Mesoporous titania-based $H_3PW_{12}O_{40}$ composite by a block copolymer surfactant-assisted templating route: preparation, characterization, and heterogeneous photocatalytic properties, Desalination 255 (2010) 107–116.
[22] A. Müller, F. Peters, M.T. Pope, D. Gatteschi, Polyoxometalates: very large clusters-nanoscale magnets, Chem. Rev. 98 (1998) 239–271.
[23] A. Dolbecq, E. Dumas, C.R. Mayer, P. Mialane, Hybrid organic–inorganic polyoxometalate compounds: from structural diversity to applications, Chem. Rev. 110 (2010) 6009–6048.
[24] C.C. Chen, W.H. Ma, J.C. Zhao, Semiconductor-mediated photodegradation of pollutants under visible-light irradiation, Chem. Soc. Rev. 39 (2010) 4206–4219.
[25] T.J. Wams, Diethylhexylphthalate as an environmental contaminant–a review, Sci. Total Environ. 66 (1987) 1–16.
[26] L. Xu, X. Yang, Y.H. Guo, F.Y. Ma, Y.N. Guo, X. Yuan, M.X. Huo, Simulated sunlight photodegradation of aqueous phthalate esters catalyzed by the polyoxotungstate/titania nanocomposite, J. Hazard. Mater. 178 (2010) 1070–1077.
[27] S. Horikoshi, F. Hojo, H. Hidaka, N. Serpone, Environmental remediation by an integrated microwave/UV illumination technique. 8. Fate of carboxylic acids, aldehydes, alkoxycarbonyl and phenolic substrates in a microwave radiation field in the presence of TiO_2 particles under UV irradiation, Environ. Sci. Technol. 38 (2004) 2198–2208.
[28] J. Ryu, W. Choi, Effects of TiO_2 surface modifications on photocatalytic oxidation of arsenite: the role of superoxides, Environ. Sci. Technol. 38 (2004) 2928–2933.
[29] S. Kim, H. Park, W. Choi, Comparative study of homogeneous and heterogeneous photocatalytic redox reactions: $PW_{12}O_{40}^{3-}$ vs TiO_2, J. Phys. Chem. B 108 (2004) 6402–6411.
[30] P.X. Lei, C.C. Chen, J. Yang, W.H. Ma, J.C. Zhao, L. Zang, Degradation of dye pollutants by immobilized polyoxometalate with H_2O_2 under visible-light irradiation, Environ. Sci. Technol. 39 (2005) 8466–8474.

[31] S.H. Yoon, J.H. Lee, Oxidation mechanism of As (III) in the UV/TiO_2 system: evidence for a direct hole oxidation mechanism, Environ. Sci. Technol. 39 (2005) 9695–9701.
[32] C.C. Chen, Q. Wang, P.X. Lei, W.J. Song, W.H. Ma, J.C. Zhao, Photodegradation of dye pollutants catalyzed by porous $K_3PW_{12}O_{40}$ under visible irradiation, Environ. Sci. Technol. 40 (2006) 3965–3970.
[33] C.S. Pan, Y.F. Zhu, New type of $BiPO_4$ oxy-acid salt photocatalyst with high photocatalytic activity on degradation of dye, Environ. Sci. Technol. 44 (2010) 5570–5574.
[34] Y.B. Xie, Photoelectrochemical reactivity of a hybrid electrode composed of polyoxophosphotungstate encapsulated in titania nanotubes, Adv. Funct. Mater. 16 (2006) 1823–1831.